Chapter 2
Establishment of a Kinetics Model

2.1 Introduction

In this chapter [1], a kinetics model for pore channel growth in anodic porous alumina during anodization is established based on the Laplacian electric potential distribution within the oxide and a continuity equation for current density within the oxide body. Both oxygen and aluminum ion current densities governed by the Cabrera–Mott equation in high electric field theory are formed by ion migration within the oxide as well as across the oxide/electrolyte (o/e) and metal/oxide (m/o) interfaces. In contrast with previous well-known oxide flow models as introduced in Chap. 1, in the present model, the movements of the o/e and m/o interfaces due to electric field-assisted oxide decomposition and metal oxidation, respectively, are governed by Faraday's law. This model can be numerically implemented by a finite element method in order to simulate the real-time evolution of the porous structure growth, which will be shown in Chap. 3.

2.2 Electric Potential Distribution Within Anodic Porous Alumina

As has been reported by Houser and Hebert [2], during anodization, space charge within anodic oxide may significantly influence the electric field distribution within the oxide region. Although space charge was considered by Dewald [3, 4] to successfully explain the experimentally observed temperature-independent Tafel slope in barrier-type anodic tantalum oxide film formation, Vermilyea [5] found that Dewald's consideration was unable to explain another experimental observation that the average electric field is independent of the anodic oxide film thickness. Thus, whether space charge should be considered during anodization still needs further investigations, and here, following Parkhutik and Shershulsky [6], Thamida

C. Cheng, *Electro-Chemo-Mechanics of Anodic Porous Alumina Nano-Honeycombs: Self-Ordered Growth and Actuation*, Springer Theses,
DOI 10.1007/978-3-662-47268-2_2

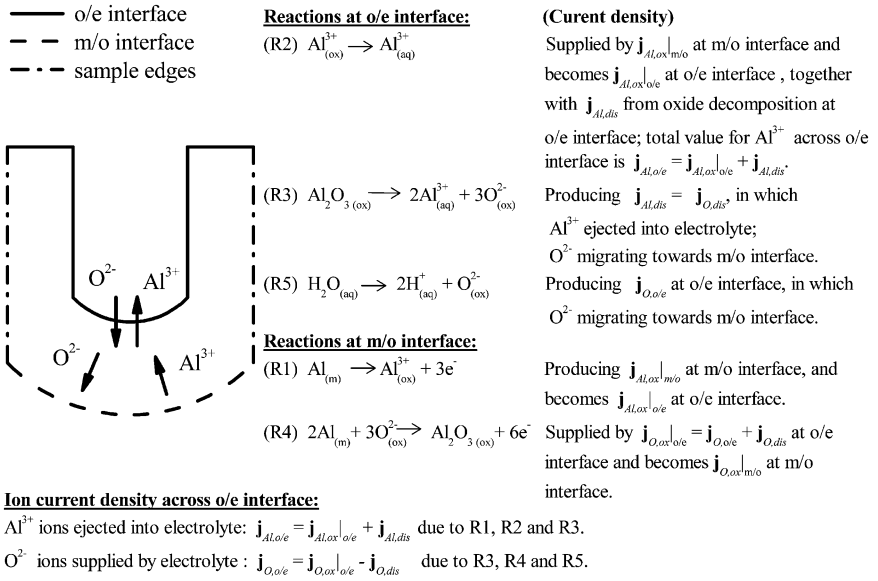

Fig. 2.1 Summary of the reactions assumed during anodic porous alumina growth. Reprinted from Ref. [1], Copyright 2011, with permission from Elsevier

and Chang [7], and Singh et al. [8, 9], we neglect space charge within the oxide. Thus, the electric potential φ within the oxide obeys the Laplace Equation

$$\nabla^2 \varphi = 0 \tag{2.1}$$

According to Houser and Hebert [2], the potential at the o/e interface (typically <0.1 V) is far smaller than the anodization voltage, and so in the present model, the potential there is set to be zero. In addition, as most of the potential drop happens within the oxide body but not in the metal substrate or in the electrolyte, the potential at the m/o interface is set to be the same as the anodization voltage V_0. In this chapter, we only investigate anodization under constant voltage conditions. Moreover, along the right and left edges of a simulation sample (e.g., the vertical dash dotted lines in Fig. 2.1), a Neumann boundary condition is used. Thus, the boundary conditions are summarized as

$$\varphi = 0, \quad \text{at o/e interface,} \tag{2.2}$$

$$\varphi = V_0, \quad \text{at m/o interface,} \tag{2.3}$$

$$\mathbf{n} \cdot \nabla \varphi = 0, \quad \text{at both edges of the sample,} \tag{2.4}$$

where $\mathbf{n}$ is the outward normal unit vector for each sample edge. The electric field is given as

$$\mathbf{E} = -\nabla \varphi. \tag{2.5}$$

The continuity requirement of the steady-state ion current density $\mathbf{j}$ within the oxide bulk can be expressed as follows [6–9]

$$\nabla \cdot \mathbf{j} = 0 \tag{2.6}$$

From the above equations, we can derive the relationship between the electric field and current density along the electric field lines across the oxide barrier layer, which will be used later. Electric field lines are always perpendicular to equipotential contours within the oxide bulk. Consider a very small cylinder with volume V_c ($V_c \to 0$), which starts from the m/o interface to the o/e interface along an electric field line across the oxide barrier layer. The top and bottom surfaces of the cylinder are elements of the o/e and m/o interfaces with areas represented as $S_{o/e}$ and $S_{m/o}$, respectively. $S_{o/e}$ and $S_{m/o}$ are not equal because of the scalloped shape of barrier layer. The side surface S_{side} of the cylinder is along the electric field line, so that its outward normal vector is perpendicular to the electric field line. From Eqs. (2.1) and (2.5), we get $\nabla \cdot \mathbf{E} = 0$, and with Gauss's Theorem $\iiint_{V_c} (\nabla \cdot \mathbf{E})\, dV = \oiint_{S_c} (\mathbf{E} \cdot \mathbf{n}) dS$, we have

$$\iint_{S_{o/e}} (\mathbf{E} \cdot \mathbf{n}) dS_{o/e} + \iint_{S_{m/o}} (\mathbf{E} \cdot \mathbf{n}) dS_{m/o} + \iint_{S_{side}} (\mathbf{E} \cdot \mathbf{n}) dS_{side} = 0. \tag{2.7}$$

Since $\mathbf{E} \cdot \mathbf{n} = 0$ over S_{side}, $\mathbf{E} = \mathbf{n} E_{o/e}$ over $S_{o/e}$, and $\mathbf{E} = -\mathbf{n} E_{m/o}$ over $S_{m/o}$, where $E_{o/e}$ and $E_{m/o}$ are the electric field intensities at $S_{o/e}$ and $S_{m/o}$, respectively, and as $S_{o/e}$ and $S_{m/o}$ both tend to zero, Eq. (2.7) becomes

$$E_{o/e} S_{o/e} = E_{m/o} S_{m/o}, \tag{2.8}$$

where $S_{o/e}$ and $S_{m/o}$ are connected by the same electric field line. By virtue of Eq. (2.6) which is of the same form as $\nabla \cdot \mathbf{E} = 0$, the above procedure can be repeated, for $\boldsymbol{j}$ to give

$$j_{o/e}S_{o/e} = j_{m/o}S_{m/o}, \tag{2.9}$$

where $j_{o/e}$ and $j_{m/o}$ are the current density magnitudes at $S_{o/e}$ and $S_{m/o}$, respectively. From Eqs. (2.8) and (2.9), we obtain

$$\frac{j_{o/e}}{j_{m/o}} = \frac{E_{o/e}}{E_{m/o}}. \tag{2.10}$$

The same derivation process actually holds for any point within the oxide bulk with electric field intensity E_{bulk} and current density j_{bulk},

$$\frac{j_*}{j_{bulk}} = \frac{E_*}{E_{bulk}}, \tag{2.11}$$

where the subscript "$_*$" represents either "o/e" or "m/o", and the oxide bulk point and the o/e or m/o interface point should be connected by the same electric field line. Equation (2.10) was first cited before by Parkhutik and Shershulsky [6], without proof, and its significance, together with that of Eq. (2.11), is as follows. For a given porous structure of anodic porous alumina, the electric field intensities can be solved directly from Eqs. (2.1–2.5). After that, regardless of whether the rate-determining step of the anodization process is at the o/e interface, oxide bulk, or m/o interface, if we can calculate the current density at one location, e.g., the o/e interface, we can obtain the current density at other two locations using Eqs. (2.10) and (2.11) directly. The location at which the current density is first evaluated may not necessarily be the location at which the rate-determining step occurs, but the calculated current density will be controlled by the rate-determining step through Eq. (2.11). Here, we assume that ion migration across the o/e interface is the rate determining step, because the oxygen and aluminum ions are weakly bound under the effect of the high electric field [10]. It should be noted that ionic migration in the bulk oxide has been proposed previously as an alternative rate determining step [11], but recent experiments revealed that an increase in the electrolyte's acid concentration, which should play a role directly at the o/e interface, can influence the anodization process significantly, such as increasing the pore diameter [12], the current density [13], and the oxide growth rate [14]. These profound changes of the anodization process should be due to anodization condition changes at the o/e interface, and this is the basis of the present assumption that the rate determining step is at this interface. In Sect. 2.3, the current density at the o/e interface is derived at first, and then the current density at the m/o interface is obtained from Eq. (2.10). Based on these, the interface movement equations are established from Faraday's Law.

2.3 Ion Migration

In anodic porous alumina formation, Cherki and Siejka's oxygen transport study using nuclear microanalyses of O^{18} and O^{16} concluded that new oxide forms only at the m/o interface but not elsewhere [15]. Also, Davies et al. [16, 17] found that Xe [18] and Rn [19] tracer distributions in barrier-type anodic alumina films formation did not tend to broaden. These experiments imply that the oxidation reaction within the oxide body is negligible. On this basis, we assume that the cations and anions migrating from one interface to another interface are not consumed on their way. On the o/e and m/o interfaces, as shown in Fig. 2.1, the most possible reactions based on previous experimental observations are described as follows:

2.3.1 Aluminum Ion Migration

Direct ejection of aluminum ions from the m/o interface into the electrolyte has been indicated in many experiments, such as coating ratio measurement and tracer experiments. The coating ratio, defined as the weight of the oxide formed to the weight of aluminum consumed in the anodization process, will be 1.89 if all of the consumed aluminum is converted into alumina, or higher if acid anions contaminate the anodic oxide, e.g., 2.2 if 14 % SO_3 contamination exists in the oxide [20]. After considering the porosity (around 10 %) [21] of the oxide due to its dissolution in the electrolyte, the coating ratio should be about 1.7 (or 1.98 if 14 % SO_3 contamination exists). However, experimentally observed values of the coating ratio are always lower. For example, Edwards and Keller [22] found that the coating ratio was smaller than about 1.46. Spooner [23] attempted to obtain a high coating ratio by increasing the current density and decreasing the dissolution rate in sulfuric acid (with SO_3 contamination in the oxide), but only 1.68 was obtained, and under other conditions the coating ratio was lower than 1.61. These imply that Al must be lost by another way beside the loss due to pore growth at the pore base assisted by the high electric field there, and this cannot be oxide dissolution loss at the pore walls or top surface, as these dissolution rates were found to be far smaller on the order of 10^{-8} cm min^{-1} [15, 24], compared with the dissolution rate of $\sim 10^{-4}$ cm/min at the pore base [23]. A similar conclusion was reached by Cherki and Siejka's O^{18} tracer experiments [15], which indicated that direct ejection of Al cations in the solution without formation of any oxide should take place. Recent experiments by Wu et al. [25] also support the net ejection of Al^{3+} cations across the barrier layer into the electrolyte. Thus, it is reasonable to assume that Al^{3+} cations formed at the m/o interface via the reaction

$$\mathrm{Al}_{(\mathrm{m})} \rightarrow \mathrm{Al}^{3+}_{(\mathrm{ox})} + 3\mathrm{e}^{-}, \tag{R1}$$

would reach the o/e interface under the drive of the high electric field, and are finally ejected into the solution by the reaction

$$\mathrm{Al}^{3+}_{(\mathrm{ox})} \rightarrow \mathrm{Al}^{3+}_{(\mathrm{aq})}, \tag{R2}$$

without oxide formation. Equation (R1) is the only source of the aluminum ions migrating through the oxide body from the m/o to e/o interface during the anodization process, and the density of such current is denoted as $\boldsymbol{j}_{\mathrm{Al,ox}}$, where "ox" means that the corresponding aluminum ions migrate through the oxide body. The value of $\boldsymbol{j}_{\mathrm{Al,ox}}$ at the m/o interface is denoted as $\boldsymbol{j}_{\mathrm{Al,ox}}|_{\mathrm{m/o}}$, while at the o/e interface is denoted as $\boldsymbol{j}_{\mathrm{Al,ox}}|_{\mathrm{o/e}}$. For anodic porous alumina formation, we must note that those aluminum ions which have traveled across the oxide barrier layer do not react to form new oxide at the o/e interface, because new oxide was found to form only at the m/o interface but not at the o/e interface [15]. The situation in barrier-type (i.e., nonporous-type) anodic alumina film formation is, however, different, since new oxide was found to form at both the m/o and o/e interfaces [16, 26]. In other words, a net aluminum current passes through the oxide barrier layer in both cases of barrier-type and porous-type alumina formation, but whether the aluminum ions reaching the o/e interface can form new oxide there would determine the type of alumina finally formed. We surmise that the acid concentration or the pH of the electrolyte would determine the fate of the aluminum ions migrated to the o/e interface, and in the model development below, this effect will be incorporated [see Eq. (2.12) later].

In addition to the direct ejection of aluminum ions, dissolution of the old oxide to form pores should take place at the o/e interface, which is thought to be also electric field assisted, because of the extremely fast dissolution rate at the pore base ($\sim 10^{-4}$ cm min^{-1}) compared with the rate at the pore walls ($\sim 10^{-8}$ cm min^{-1}) as found in experiments [15, 24]. Such a great difference in the dissolution rates should be mainly due to the large difference in electric field intensities between these two locations. Furthermore, Siejka and Ortega's O^{18} tracer experiments [27] showed that oxygen loss during pore formation is negligible, which would contradict the dissolution reaction $\mathrm{Al_2O_{3(ox)}} + 6\mathrm{H}^{+}_{(\mathrm{aq})} \rightarrow 2\mathrm{Al}^{3+}_{(\mathrm{aq})} + 3\mathrm{H_2O_{(aq)}}$ assumed in some previous studies [7, 28], since this reaction would involve loss of oxygen from the oxide into the electrolyte. Instead, the old oxide at pore base is likely to be consumed by the following decomposition reaction [27]:

$$\mathrm{Al_2O_{3(ox)}} \rightarrow 2\mathrm{Al}^{3+}_{(\mathrm{aq})} + 3\mathrm{O}^{2-}_{(\mathrm{ox})}, \tag{R3}$$

in which the product oxygen remains in the oxide body, and is then driven by the high electric field to reach the m/o interface to form new oxide there. Thus, the so-called "field-assisted dissolution of oxide" referred to by some previous researchers [10, 29, 30] is interpreted here as the field-assisted decomposition of oxide at the o/e interface. Let $\boldsymbol{j}_{\mathrm{O,dis}}$ and $\boldsymbol{j}_{\mathrm{Al,dis}}$ denote the oxygen ion and aluminum ion current density due to (R3) at the o/e interface. Their values are equal, but the corresponding ion movements are in opposite directions, i.e.,

$$\boldsymbol{j}_{\mathrm{Al,dis}} = \boldsymbol{j}_{\mathrm{O,dis}}. \tag{2.12}$$

The experimentally established field-assisted ejection of aluminum ions into the electrolyte, the current density of which is denoted as $\boldsymbol{j}_{\mathrm{Al,o/e}}$ hereafter, is contributed by aluminum ions produced by oxide decomposition at the o/e interface [of current density $\boldsymbol{j}_{\mathrm{Al,dis}}$ in (R3)], as well as ions migrated from the m/o interface [of current density $\boldsymbol{j}_{\mathrm{Al,ox}}|_{\mathrm{o/e}}$ in (R2)], i.e.,

$$\boldsymbol{j}_{\mathrm{Al,o/e}} = \boldsymbol{j}_{\mathrm{Al,ox}}\big|_{\mathrm{o/e}} + \boldsymbol{j}_{\mathrm{Al,dis}}. \tag{2.13}$$

At the o/e interface, although the aluminum ions ejected into the electrolyte come from two sources, the actual ejection process which is reaction (R2) has no difference from an electrolyte point of view. Physically, this process is governed by the high-field theory [31–33] in which the aluminum ions are assumed to jump across a potential barrier W_{Al} at the o/e interface, the effective value of which is reduced by an amount $\alpha_{\mathrm{Al}} a_{\mathrm{Al}} q_{\mathrm{Al}} E_{\mathrm{o/e}}$ in the jumping direction along the electric field $E_{\mathrm{o/e}}$, and increased by $(1 - \alpha_{\mathrm{Al}}) a_{\mathrm{Al}} q_{\mathrm{Al}} E_{\mathrm{o/e}}$ in the opposite direction. Thus, the $\boldsymbol{j}_{\mathrm{Al,o/e}}$ can be expressed as the Cabrera–Mott equation [32],

$$\boldsymbol{j}_{\mathrm{Al,o/e}} = \left\{ n_{\mathrm{Al}} q_{\mathrm{Al}} v_{\mathrm{Al}} \exp\left(-\frac{W_{\mathrm{Al}} - \alpha_{\mathrm{Al}} q_{\mathrm{Al}} a_{\mathrm{Al}} E_{\mathrm{o/e}}}{kT} \right) - n_{\mathrm{Al}} q_{\mathrm{Al}} v_{\mathrm{Al}} \exp\left[-\frac{W_{\mathrm{Al}} + (1 - \alpha_{\mathrm{Al}}) q_{\mathrm{Al}} a_{\mathrm{Al}} E_{\mathrm{o/e}}}{kT} \right] \right\} \hat{\mathbf{E}}_{\mathrm{o/e}}, \tag{2.14}$$

where n_{Al} is the surface density of mobile aluminum ions at the o/e interface which is dependent on electric intensity [4], q_{Al} is the charge of one aluminum ion, v_{Al} is the vibration frequency of aluminum ions, α_{Al} is a transfer coefficient related to the symmetry of the potential barrier (e.g., if the potential barrier is symmetrical, then $\alpha_{\mathrm{Al}} = 0.5$), a_{Al} is the jump distance (twice the activation distance) of aluminum ions, $\mathbf{E}_{\mathrm{o/e}}$ is the electric field at o/e interface, $E_{\mathrm{o/e}} = |\mathbf{E}_{\mathrm{o/e}}|$ is the electric field intensity, $\hat{\mathbf{E}}_{\mathrm{o/e}}$ is the unit vector $\mathbf{E}_{\mathrm{o/e}}/E_{\mathrm{o/e}}$, k is the Boltzmann constant, and T is the absolute temperature. The Cabrera–Mott equation above contains terms that describe jumps in both the forward and backward directions, but in practice, the backward current density (the second term in Eq. 2.14) is far smaller than the forward one (the first term in Eq. 2.14) [33], and so to save computation time only the forward current

was considered in the present numerical simulations. Furthermore, following Diggle [30] and Vermilyea [34], to describe the fact that the dissolution process is strongly influenced by the acid concentration C_{H^+}, the current density is scaled by the factor $(C_{H^+})^{\eta}$, where $\eta = \alpha/\varsigma \in [0, 1]$ is the ratio of the number of protons α involved in the dissolution process to the stoichiometric number ς appropriate to the dissolution mechanism [30]. This power term $(C_{H^+})^{\eta}$ was also used in previous reports [6–9]. Diggle [30] stated that only the current of the ion species involved in the rate determining process should be scaled by $(C_{H^+})^{\eta}$, and here we believe that aluminum ions rather than oxygen ions are more likely the rate controlling species, since, as discussed above, aluminum ions need to jump across a high potential barrier at the o/e interface to enter the electrolyte, while oxygen ions migrate within the oxide body toward the m/o interface, and such migration can take place along some easy paths such as microchannels [15, 35, 36] or by vacancy motion [28]. Thus, after neglecting the backward current density and scaling the current density by the acid concentration in Eq. (2.14), the total aluminum ion current which goes into the electrolyte is given as

$$\boldsymbol{j}_{\mathrm{Al,o/e}} = n_{\mathrm{Al}} A_{\mathrm{Al}} \exp(k_{\mathrm{Al}} E_{\mathrm{o/e}}) \hat{\mathbf{E}}_{\mathrm{o/e}}, \tag{2.15}$$

where $A_{\mathrm{Al}} = C_{H^+}^{\eta} q_{\mathrm{Al}} v_{\mathrm{Al}} \exp(-W_{\mathrm{Al}}/kT)$ and $k_{\mathrm{Al}} = \alpha_{\mathrm{Al}} q_{\mathrm{Al}} a_{\mathrm{Al}}/kT$.

2.3.2 Oxygen Ion Migration

According to Cherki and Siejka's oxygen transport study [15], new oxide is only formed at the m/o interface, but not at the electrolyte/barrier layer interface or at the outer surface of the porous film. This means that O^{2-} ions have to migrate from the o/e interface to the m/o interface across the barrier layer under the high electric field. Once the oxygen ions reach the m/o interface, the following reaction may take place:

$$2\mathrm{Al}_{(\mathrm{m})} + 3\mathrm{O}^{2-}_{(\mathrm{ox})} \rightarrow \mathrm{Al_2O_{3(ox)}} + 6\mathrm{e}^{-}. \tag{R4}$$

Equation (R4) accounts for the entire migration of oxygen ions through the oxide body, the current density of which is denoted as $\boldsymbol{j}_{\mathrm{O,ox}}$, where "ox" again means that the current goes through the oxide body, and the local value of $\mathbf{j}_{\mathrm{O,ox}}$ at the m/o interface is denoted as $\boldsymbol{j}_{\mathrm{O,ox}}|_{\mathrm{m/o}}$, while that at the o/e interface is denoted as $\boldsymbol{j}_{\mathrm{O,ox}}|_{\mathrm{o/e}}$. In turn $\boldsymbol{j}_{\mathrm{O,ox}}|_{\mathrm{o/e}}$ is contributed by two sources of oxygen ions: one is from water decomposition at the o/e interface [37]

$$H_2O_{(aq)} \rightarrow 2H^+_{(aq)} + O^{2-}_{(ox)}. \tag{R5}$$

the current density of which is denoted as $\boldsymbol{j}_{O,o/e}$, and the other source is from decomposition of old oxide at the o/e interface by reaction (R3), the current density of which is $\boldsymbol{j}_{O,dis}$ which is equal to $\boldsymbol{j}_{Al,dis}$ (Eq. 2.12). Thus,

$$\boldsymbol{j}_{O,ox}\big|_{o/e} = \boldsymbol{j}_{O,o/e} + \boldsymbol{j}_{O,dis}. \tag{2.16}$$

As stated in Sect. 2.3.1, after oxide decomposition according to (2.14), the product aluminum ions will jump across the o/e interface to enter the electrolyte, while the oxygen ions will not cross that potential barrier but will migrate toward the m/o interface by some easy paths. Thus, only those oxygen ions coming from water decomposition [with current density $\boldsymbol{j}_{O,o/e}$ from (R5)] need to jump across the potential barrier at the o/e interface, and this current density should also follow the Cabrera–Mott equation [32]. By neglecting the backward current density which is small, $\boldsymbol{j}_{O,o/e}$ is given as

$$\boldsymbol{j}_{O,o/e} = n_O A_O \exp(k_O E_{o/e}) \hat{\mathbf{E}}_{o/e}, \tag{2.17}$$

where $A_O = q_O v_O \exp(-W_O/kT)$ and $k_O = \alpha_O q_O a_O/kT$, and the parameters in these expressions have similar meanings as in Eq. (R3) albeit now for oxygen ions. From Eqs. (2.15) and (2.16), the total ion current density which will go across the o/e interface is

$$\boldsymbol{j}_{total,o/e} = \boldsymbol{j}_{Al,o/e} + \boldsymbol{j}_{O,o/e} = \left[n_{Al} A_{Al} \exp\left(k_{Al} E_{o/e}\right) + n_O A_O \exp\left(k_O E_{o/e}\right)\right] \hat{\mathbf{E}}_{o/e}. \tag{2.18}$$

It should be emphasized that in the present model, the oxide body is assumed to be the channel for ion migration, and ions are assumed not able to accumulate or be neutralized. As mentioned above, we also assume that jumps of ions across the o/e interface is the rate determining step for their entire migration across the oxide body, where the oxygen and aluminum ions are weakly bound under the effect of the high electric field, in accordance with O'Sullivan and Wood's field-assisted dissolution theory [10].

2.3.3 Relationship Between Aluminum Ion Current Density and Oxygen Ion Current Density Within the Oxide Body

According to the discussion in Sects. 2.3.1 and 2.3.2, continuous growth of porous alumina depends on the outward migration of aluminum ions (with current density $\boldsymbol{j}_{\mathrm{Al,ox}}$) and inward migration of oxygen ions (with current density $\boldsymbol{j}_{\mathrm{O,ox}}$) across the oxide barrier layer. We propose that these two current densities should have a fixed relationship because of the following reason. During anodization, many experiments have proven that the metal substrate and the oxide barrier layer are in good contact with each other [10], although the theoretical volume expansion ratio (the Pilling–Bedworth ratio) [28, 38, 39] equals to 1.7 at the m/o interface. This implies that the oxygen ions must be provided with enough spaces at the m/o interface to form new oxide without influencing the close contact between metal and oxide. These spaces can only be due to the ejected aluminum ions from the m/o interface which will migrate across the oxide barrier layer. As the volume expansion accompanying the oxidation reaction at the m/o interface is fixed under a certain anodization condition, the required spaces to accommodate such volume expansion for maintaining good metal oxide contact is then fixed, and so the ratio between the outward amount of aluminum ion current density and the inward amount of oxygen ion current density,

$$\beta = \frac{j_{\mathrm{Al,ox}}\big|_{\mathrm{m/o}}}{j_{\mathrm{O,ox}}\big|_{\mathrm{m/o}}} = \frac{j_{\mathrm{Al,ox}}\big|_{\mathrm{o/e}}}{j_{\mathrm{O,ox}}\big|_{\mathrm{o/e}}}, \tag{2.19}$$

should also be fixed during anodization, where $j_{\mathrm{Al,ox}}|_{\mathrm{m/o}} = |\boldsymbol{j}_{\mathrm{Al,ox}}|_{\mathrm{m/o}}|$, $j_{\mathrm{O,ox}}|_{\mathrm{m/o}} = |\boldsymbol{j}_{\mathrm{O,ox}}|_{\mathrm{m/o}}|$, $j_{\mathrm{Al,ox}}|_{\mathrm{o/e}} = |\boldsymbol{j}_{\mathrm{Al,ox}}|_{\mathrm{o/e}}|$, and $j_{\mathrm{O,ox}}|_{\mathrm{o/e}} = |\boldsymbol{j}_{\mathrm{O,ox}}|_{\mathrm{o/e}}|$. In Eq. (2.19), "ox" means that the corresponding ions migrate across the oxide, and $|_{\mathrm{m/o}}$ and $|_{\mathrm{o/e}}$ mean that the values of the corresponding current densities are at the m/o or o/e interfaces, respectively. In achieving the second step in Eq. (2.19), a continuity condition

$$j_{,\mathrm{ox}}\big|_{\mathrm{m/o}} = j_{,\mathrm{ox}}\big|_{\mathrm{o/e}} \frac{E_{\mathrm{m/o}}}{E_{\mathrm{o/e}}} \tag{2.20}$$

linking the current densities $\boldsymbol{j}_{,\mathrm{ox}}|_{\mathrm{m/o}}$ and $\boldsymbol{j}_{,\mathrm{ox}}|_{\mathrm{o/e}}$ at two points on the m/o and o/e interfaces connected by the same electric field line is used for both ion species, noting that the electric field intensities at the two points $E_{\mathrm{m/o}} = |\mathbf{E}_{\mathrm{m/o}}|$ and $E_{\mathrm{o/e}} = |\mathbf{E}_{\mathrm{o/e}}|$ are common for both species. Equation (2.20) comes from Eq. (2.10) derived in Sect. 2.2. From Eqs. (2.12), (2.13), (2.16), and (2.19), and noting that $\boldsymbol{j}_{\mathrm{Al,ox}}|_{\mathrm{o/e}}$, $\boldsymbol{j}_{\mathrm{O,ox}}|_{\mathrm{o/e}}$, $\boldsymbol{j}_{\mathrm{Al,o/e}}$, $\boldsymbol{j}_{\mathrm{O,o/e}}$, $\boldsymbol{j}_{\mathrm{Al,dis}}$, and $\boldsymbol{j}_{\mathrm{O,dis}}$ have the same direction $\hat{\mathbf{E}}_{\mathrm{o/e}}$ at a given point on o/e interface,

$$\mathbf{j}_{\mathrm{Al,dis}} = \frac{j_{\mathrm{Al,o/e}} - \beta j_{\mathrm{O,o/e}}}{1+\beta}\hat{\mathbf{E}}_{\mathrm{o/e}}, \tag{2.21}$$

where $j_{\mathrm{Al,dis}} = |\mathbf{j}_{\mathrm{Al,dis}}|$. Strictly speaking, under different anodization conditions such as voltage, electrolyte type, concentration, or substate grain orientation, β may change a little because the volume expansion ratio may change, but the change is expected to be small as the oxide density is usually around 3 g/cm^3 from experiments [4, 40]. An example of substrate grain orientation dependence of β will be shown in Chap. 5. As a typical condition, we set β to be 3/7 in accordance with Siejka and Ortega's experimental results [27]. It should also be noted that the β defined in Eq. (2.19) is not the same as the current efficiency $\mu = j_{\mathrm{O,o/e}}/(j_{\mathrm{O,o/e}} + j_{\mathrm{Al,o/e}})$, and so a constant β does not mean that the current efficiency is also a constant.

2.4 Interface Movement Equations

From Faraday's law [1], the change in volume V of the oxide caused by a passed charge Q carried by ions is

$$V = \frac{MQ}{zF\rho} = \frac{MAjt}{zF\rho}, \tag{2.22}$$

where M is the molecular weight of oxide $\mathrm{Al}_x\mathrm{O}_y$, $z = xy$, ρ is the oxide density, j is the amount of current density corresponding to the reaction, A is the area of oxide surface, t is time and F is Faraday's constant. Thus, the moving velocity $\mathbf{v}$ of the oxide thickness $D = V/A$ at a given point at the interface is proportional to the current density as

$$\mathbf{v} = -\frac{\mathrm{d}D}{\mathrm{d}t}\hat{\mathbf{E}} = -\frac{M}{zF\rho}j\hat{\mathbf{E}}. \tag{2.23}$$

where $\hat{\mathbf{E}} = \mathbf{E}/E$ is the unit vector of the electric field at that given point on the interface. Equation (2.23) is not only suitable for the m/o interface where the oxidation reaction R4 takes place but is also suitable for the o/e interface movement where the oxide decomposition reaction (R3) takes place. The moving velocity direction is in the opposite direction of the electric field at a given point on the interface. More specifically, at the o/e interface, the interface movement velocity is $\mathbf{v}_{\mathrm{o/e}} = -\mathbf{j}_{\mathrm{Al,dis}}M/zF\rho$, and substituting in Eq. (2.21), and replacing $\mathbf{j}_{\mathrm{Al,o/e}}$ and $\mathbf{j}_{\mathrm{O,o/e}}$ by Eqs. (2.15) and (2.17), respectively, we obtain

$$\mathbf{v}_{\mathrm{o/e}} = -\frac{M}{zF\rho(1+\beta)}\left[n_{\mathrm{Al}}A_{\mathrm{Al}}\exp(k_{\mathrm{Al}}E_{\mathrm{o/e}}) - \beta\, n_{\mathrm{o}}A_{\mathrm{o}}\exp(k_{\mathrm{o}}E_{\mathrm{o/e}})\right]\hat{\mathbf{E}}_{\mathrm{o/e}}. \tag{2.24}$$

Similarly, the m/o interface movement velocity is $\mathbf{v}_{m/o} = -\mathbf{j}_{O,ox}|_{m/o} M/zF\rho$, and from Eqs. (2.12), (2.16), (2.15), (2.17), (2.20), and (2.21), this is given as

$$\mathbf{v}_{m/o} = -\frac{M}{zF\rho(1+\beta)}\frac{E_{m/o}}{E_{o/e}}\left[n_{Al}A_{Al}\exp\left(k_{Al}E_{o/e}\right) + n_O A_O \exp\left(k_O E_{o/e}\right)\right]\hat{\mathbf{E}}_{m/o}. \tag{2.25}$$

where $\hat{\mathbf{E}}_{m/o} = \mathbf{E}_{m/o}/E_{m/o}$. In Eq. (2.25), as in Eq. (2.20), the two electric field intensities $E_{m/o}$ and $E_{o/e}$ are those at two points on the m/o and o/e interfaces connected by a given electric field line. It should also be noted that, although Eq. (2.25) is for the velocity of the m/o interface, the present formalism is such that the parameters n_{Al}, n_O, A_{Al}, A_O, k_{Al}, and k_O all refer the o/e interface where the rate-determining energy barrier exists.

2.5 Summary

In this chapter [1], a kinetics model for pore channel growth in anodic porous alumina has been established based on the Laplacian electric potential distribution within the oxide and the high electric field transport theory for ions. In contrast with the previous oxide flow model [41–51] in which pores were assumed to form by oxide flow from the pore bases to pore walls driven by mechanical stresses, in our model, pores are formed by electric field-assisted oxide decomposition at the o/e interface and oxide formation at the m/o interface.

References

1. C. Cheng, A.H.W. Ngan, Electrochim. Acta **56**, 9998 (2011)
2. J.E. Houser, K.R. Hebert, J. Electrochem. Soc. **153**, B566 (2006)
3. J.F. Dewald, Acta. Met. **2**, 340 (1954)
4. J.F. Dewald, J. Electrochem. Soc. **102**, 1 (1955)
5. D.A. Vermilyea, Acta Met. **1**, 282 (1953)
6. V.P. Parkhutik, V.I. Shershulsky, J. Phys. D Appl. Phys. **25**, 1258 (1992)
7. S.K. Thamida, H.C. Chang, Chaos **12**, 240 (2002)
8. G.K. Singh, A.A. Golovin, I.S. Aranson, V.M. Vinokur, Europhys. Lett. **70**, 836 (2005)
9. G.K. Singh, A.A. Golovin, I.S. Aranson, Phys. Rev. B **73**, 205422 (2006)
10. J.P. O'Sullivan, G.C. Wood, Proc. R. Soc. Lond. A **317**, 511 (1970)
11. G. Patermarakis, J. Electroanal. Chem. **635**, 39 (2009)
12. N.Q. Zhao, X.X. Jiang, C.S. Shi, J.J. Li, Z.G. Zhao, X.W. Du, J. Mater. Sci. **42**, 3878 (2007)
13. S. Ono, M. Saito, M. Ishiguro, H. Asoh, J. Electrochem. Soc. **151**, B473 (2004)
14. A.L. Friedman, D. Brittain, L. Menon, J. Chem. Phys. **127**, 154717 (2007)
15. C. Cherki, J. Siejka, J. Electrochem. Soc. **120**, 784 (1973)
16. J.A. Davies, B. Domeij, J.P.S. Pringle, F. Brown, J. Electrochem. Soc. **112**, 675 (1965)

17. J.A. Davies, B. Domeij, J. Electrochem. Soc. **110**, 849 (1963)
18. T.P. Hoar, N.F. Mott, J. Phys. Chem. Solids **9**, 97 (1959)
19. T. Valand, K.E. Heusler, J. Electroanal. Chem. **149**, 71 (1983)
20. J.W. Diggle, T.C. Downie, C.W. Goulding, Chem. Rev. **69**, 365 (1969)
21. K. Nielsch, J. Choi, K. Schwim, R.B. Wehrspohn, U. Gösele, Nano Lett. **2**, 677 (2002)
22. J.D. Edwards, F. Keller, Trans. Electrochem. Soc. **79**, 180 (1940)
23. R.C. Spooner, J. Electrochem. Soc. **102**, 156 (1955)
24. M. Nagayama, K. Tamura, Electrochim. Acta **12**, 1097 (1967)
25. Z. Wu, C. Richter, L. Menon, J. Electrochem. Soc. **154**, E8 (2007)
26. J.L. Whitton, J. Electrochem. Soc. **115**, 58 (1968)
27. J. Siejka, C. Ortega, J. Electrochem. Soc. **124**, 883 (1977)
28. F. Li, L. Zhang, R.M. Metzger, Chem. Mater. **10**, 2470 (1998)
29. G.C. Wood, in *Oxide and Oxide Films*, vol. 2, ed. by J.W. Diggle (Marcel Dekker, New York, 1973), p. 167
30. J.W. Diggle, in *Oxide and Oxide Films*, vol. 2, ed. by J.W. Diggle (Marcel Dekker, New York, 1973), p. 281
31. M.M. Lohrengel, Mater. Sci. Eng. R **11**, 243 (1993)
32. N. Cabrera, N.F. Mott, Rep. Prog. Phys. **12**, 163 (1949)
33. L. Young, *Anodic Oxide Films* (Academic Press, London, 1961)
34. D.A. Vermilyea, J. Electrochem. Soc. **113**, 1067 (1966)
35. G.A.J. Dorsey, J. Electrochem. Soc. **113**, 169 (1966)
36. L. Vecchia, G. Piazzesi, F. Siniscalco, Electrochim. Metal **2**, 71 (1967)
37. J. Siejka, J.P. Nadai, G. Amsel, J. Electrochem. Soc. **118**, 727 (1970)
38. N.B. Pilling, R.E. Bedworth, J. Inst. Metals **29**, 529 (1923)
39. R.E. Smallman, A.H.W. Ngan, *Physical Metallurgy and Advanced Materials* (Elsevier, Amsterdam, 2007)
40. S. Lee, H.S. White, J. Electrochem. Soc. **151**, B479 (2004)
41. J.E. Houser, K.R. Hebert, Phys. Status Solidi (a) **205**, 2396 (2008)
42. J.E. Houser, K.R. Hebert, Nat. Mater. **8**, 415 (2009)
43. S.J. Garcia-Vergara, T. Hashimoto, P. Skeldon, G.E. Thompson, H. Habazaki, Electrochim. Acta **54**, 3662 (2009)
44. S.J. Garcia-Vergara, L. Iglesias-Rubianes, C.E. Blanco-Pinzon, P. Skeldon, G.E. Thompson, P. Campestrini, Proc. R. Soc. A **462**, 2345 (2006)
45. S.J. Garcia-Vergara, P. Skeldon, G.E. Thompson, H. Habazaki, Electrochim. Acta **52**, 681 (2006)
46. S.J. Garcia-Vergara, P. Skeldon, G.E. Thompson, H. Habazaki, Thin Solid Films **515**, 5418 (2007)
47. S.J. Garcia-Vergara, P. Skeldon, G.E. Thompson, H. Habazaki, Corros. Sci. **50**, 3179 (2008)
48. S.J. Garcia-Vergara, P. Skeldon, G.E. Thompson, T. Hashimoto, H. Habazaki, J. Electrochem. Soc. **154**, C540 (2007)
49. P. Skeldon, G.E. Thompson, S.J. Garcia-Vergara, L. Iglesias-Rubianes, G.E. Blanco-Pinzon, Electrochem. Solid State Lett. **9**, B47 (2006)
50. S.J. Garcia-Vergara, P. Skeldon, G.E. Thompson, H. Habazaki, Corros. Sci. **49**, 3772 (2007)
51. S.J. Garcia-Vergara, P. Skeldon, G.E. Thompson, H. Habazaki, Surf. Inerface Anal. **39**, 860 (2007)

http://www.springer.com/978-3-662-47267-5

Electro-Chemo-Mechanics of Anodic Porous Alumina Nano-Honeycombs: Self-Ordered Growth and Actuation

Cheng, C.

2015, XVII, 278 p. 70 illus., 49 illus. in color., Hardcover
ISBN: 978-3-662-47267-5